HIGH CONCENTRATION THULIUM-DOPED GERMANATE LASERS AND AMPLIFIERS

by

Patrick Keiffer

A Thesis Submitted to the Faculty of the

COLLEGE OF OPTICAL SCIENCES

In Partial Fulfillment of the Requirements

For the Degree of

MASTER OF SCIENCE

In the Graduate College

THE UNIVERSITY OF ARIZONA

2019

THE UNIVERSITY OF ARIZONA
GRADUATE COLLEGE

As members of the Master's Committee, we certify that we have read the thesis prepared by: *Patrick Keiffer*

titled: *HIGH CONCENTRATION THULIUM –DOPED GERMANATE LASERS AND AMPLIFIERS*

and recommend that it be accepted as fulfilling the thesis requirement for the Master's Degree.

[Committee Chair Name: Nasser Peyghambarian Date: 11/18/19

[Committee Member Name:Xiushan Zhu Date: 11/18/19

[Committee Member Name] : Pierre Blanche Date: 11/18/19

[Committee Member Name] : Arturo Chavez-Pirson Date: 11/18/19

Final approval and acceptance of this thesis is contingent upon the candidate's submission of the final copies of the thesis to the Graduate College.

I hereby certify that I have read this thesis prepared under my direction and recommend that it be accepted as fulfilling the Master's requirement.

Date: 11/18/19

[Co Nasser Peyghambarian
Master's Thesis Committee Chair
College of Optical Sciences

Acknowledgments

I would first like to take the time to recognize the immense support and guidance I have received during my graduate school experience. This journey has been a long and challenging one and I could not have done it without help from a strong support structure. I would first like to thank my advisor, Dr. Nasser Peyghambarian. You have always believed in my capabilities as a scientist and provided me with the chance to perform research at the highest level. I am forever thankful for the opportunities you have given me. I would also like to thank Dr. Xiushan Zhu, who has always been willing to answer my questions and provide research guidance. The vast majority of my understanding of fiber lasers occurred under his guidance. I would like to thank Dr. Arturo Chavez-Pirson and Holly Griffin who have helped mold me into a better team player and have always encouraged me to grow stronger in areas I was weak. I would like to thank my lab mates throughout the years, specifically Minghong Tong and Ricky Gibson. I was lucky enough to work underneath their guidance and their mentorship has been invaluable to me. They were both extremely patient with me and I consider them to be true friends. Finally, I would like to thank my friends and family, specifically my parents, Richard and Lourdes, my sister Cristina, and my partner Michelle Coe. You four could not begin to understand the amount of strength and encouragement you have provided me over these years and I draw inspiration from you every day.

Dedication

This thesis is dedicated to my grandfather, Dr. David Goforth Keiffer Jr., the strongest man I have ever met and the first of three generations of physicist. I pray that I can inspire others the way my grandfather inspired me.

Contents

List of Figures

Abstract

A thulium-doped germanate fiber laser and thulium-doped germanate slab amplifier are developed their benefits to relevant applications is discussed. The fiber laser has a single spatial mode and a single transverse cavity mode with a center wavelength of 1978nm. A commercial production-ready prototype was developed during this work. The slab amplifier is designed for high energy amplification applications where all-fiber solutions fall short. The slab laser as presented here was unable to successfully see gain due to thermal limitations, but with further work is still a promising approach for pulse energy scaling in a glass medium. Modeling results of the slab amplifier are presented here.

Chapter 1

Introduction

Laser systems have become an undeniably critical technology in our everyday life. From Gordan Gould sketching the first optical resonator for coherent radiation in 1959 to today, the laser industry has grown to a whopping $14.60B USD industry. With such clear demand, the hunt for new applications and improvements in technology is never-ending. Part of this exploration is to advance source technology for wavelengths of interest. In the last decade, Thulium (Tm)-doped media, which provide "eye-safe" radiation in the 1.9um to 2μm range, has proven to be of great interest [4]. This wavelength range is attractive to many applications including spectroscopy, medical procedures, material processing, and military countermeasures [3]. In this thesis, I discuss my efforts to expand optical fiber-based source capabilities in form and function in the 1.9μm to 2μm wavelength range using highly doped Thulium-Germanate optical fiber provided by NP Photonics.

1.1 History

The fundamental physics behind laser technology was first predicted by Albert Einstein in 1917 [5]. Einstein theorized that not only could electromagnetic (EM) radiation cause an electron to be excited to a higher atomic level, but it could also encourage the decay of an electron into a lower state. Conservation of energy would then require that each decay event would result in the emission of a quantized unit of EM energy called a photon from the atom. These photons would have characteristic oscillation frequencies equal to the energy difference between the excited state and ground state. Some 40 years later, researchers Gordon Gould, Arthur Schawlow, and Charles Townes first described how to build an optical cavity to harness and amplify these emitted photons, calling it a LASER or Light Amplification by Stimulated Emission of Radiation. It wasn't long after that Theodore Maiman built the first laser in May of 1960 and thus a new chapter in physics had begun. Over the next 60 years, the field of laser physics would see continual innovation, making lasers present in almost every aspect of everyday life.

1.2 Areas of Interest

2μm laser systems exist in a class of lasers called "eye-safe". This is due to the strong water absorption in this region. "Eye-safe" is somewhat of a misnomer and really refers to retina safe. An "eye-safe" laser, when shone into an eye, sees significant absorption in the cornea, preventing the retina from being damaged. The result is that the damage done is repairable and thus "safe". This "eye-safe" quality makes these lasers of particular interest in

military applications where friendly and enemy combatants could be blinded by a sweeping laser [6].

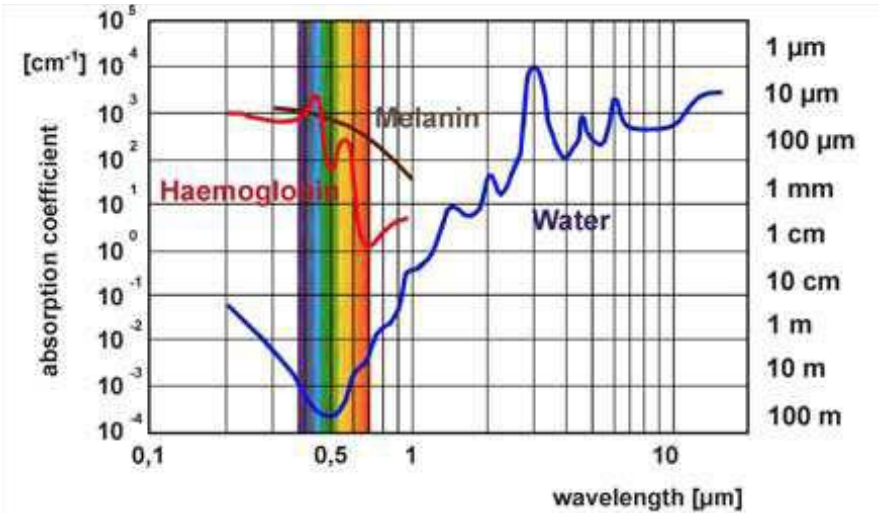

Fig. 1. *Absorption of light in water and other biological tissue [3].*

The large absorption in water is also very attractive to medical applications. 2μm laser sources are ideal for precision surgery applications since human tissue is majority water. Not only does this result in a small damage region, but the selective absorption of hemoglobin in this region can cause blood to coagulate when exposed to light at 2μm [3].

Another important application of 2μm lasers is in the world of material processing. Laser welding is a well-established market; however, plastic welding in particular has struggled to find a quality laser source. Many plastic materials are transparent in the 1μm range where the majority of commercial laser systems operate. To combat this transparency, many manufacturers work with plastics that have additives increasing the absorption in the 1μm band. 2μm, however, is highly absorbed in most plastics making it an ideal source for high precision plastic welding. 2μm laser light can be focused so that the intensity of light is only high enough to melt a region

of interest. In the future, 2μm laser plastic welding will facilitate the advancement of plastic medical devices where high-precision, micro-welds are needed [2].

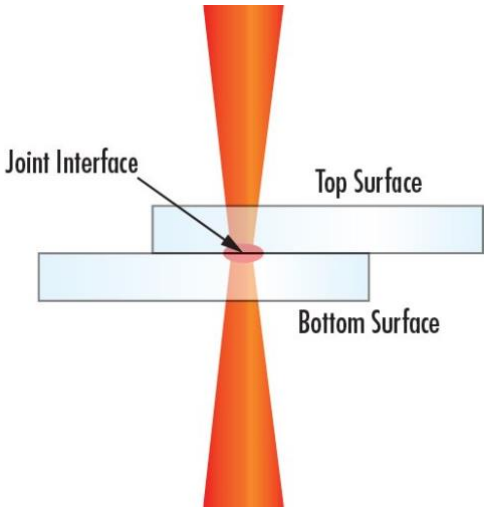

Fig. 2. *Plastic welding using 2μm laser [2].*

1.3 Thulium Germanate as a Gain Media

Thulium is an optically active, trivalent rare-earth element commonly used as a dopant for lasers operating in the 2μm range. Rare-earth elements are a class of fifteen elements that all display electronic structures with weakly allowed transitions that can be exploited for use as gain media in laser and amplifier systems [7]. Unlike other optically active ions, trivalent rare-earth ions have electronic structures that shield the electrons in the 4F shell from the local Coulombic environment [8]. This results in weakly allowed transitions and relatively long upper-state lifetimes [9]. This shield also makes rare-earth ion transitions strongly absorptive and less sensitive to host material [10].

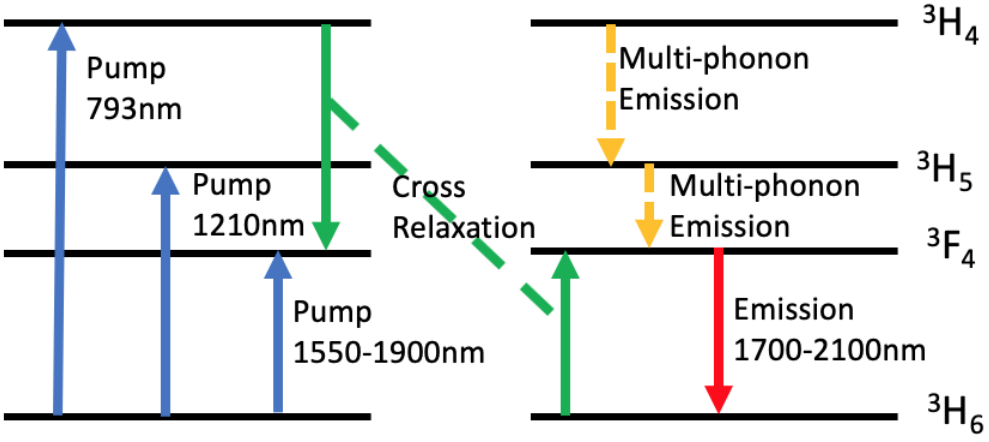

Fig. 3. *Diagram of Tm^{3+} Energy Levels.*

The relevant energy levels of Thulium, depicted in Figure 3, show convenient absorption resonances at 793nm, 1210nm, and 1570nm. This makes Thulium an attractive 2μm source with plenty of inexpensive, commercially available, high-power pump laser options. The broad emission spectra is also attractive for tunable 2μm laser sources. Another attractive characteristic of Tm^{3+} is the presence of a mechanism called cross-relaxation. Cross-relaxation is a process that occurs when one excited and one ground state Thulium atom are close enough to one another. The Tm^{3+} atom in the ground state ($^3H_6$) gets excited to the upper laser level ($^3F_4$) by absorbing the energy from the neighboring atom that underwent decay from $^3H_4$ level to the $^3F_4$ level. When this phenomenon occurs, two ground state ($^3H_6$) atoms get excited to the $^3F_4$ level for each photon at 793nm. This results in a quantum efficiency greater than one making pumping at 793nm more attractive than pumping at 1210nm or 1570nm [11].

With this phenomenon in mind, the naïve approach would be to attempt to dope a host media with as much Thulium ions as possible. However, in reality, clustering effects of

neighboring ions start to reduce the laser and amplifier efficiency as concentration increases. If ion concentration is high enough, neighboring ions will electronically communicate and transfer energy from one ion to the other. This results in the second ion gaining an electron in the excited state while the original ion non-radiatively decays to the ground state. Thus, for every cluster of two, only half of the ions are in an excited state and able to contribute to the lasing process regardless of pump power [12]. Higher doping concentrations lead to higher clustering probabilities and thus truncating the potential lasing efficiency. This effect is often referred to as concentration quenching.

1.4 Germanate as a Host Media

One way to avoid concentration quenching is to select a host media that has high solubility. A higher gain ion solubility will allow for higher doping concentrations while avoiding quenching effects. Heavy metal oxide glasses like germanate glass have high thulium ion solubility compared to silica glasses [13]. Additionally, germanate has a low phonon energy ($900cm^{-1}$) which helps lower the non-radiative decay rate of the upper lasing level [13]. NP Photonics has managed to dope germanate fiber with thulium to a 4% weight concentration. This glass was used in both the single-frequency laser and slab amplifier research discussed here.

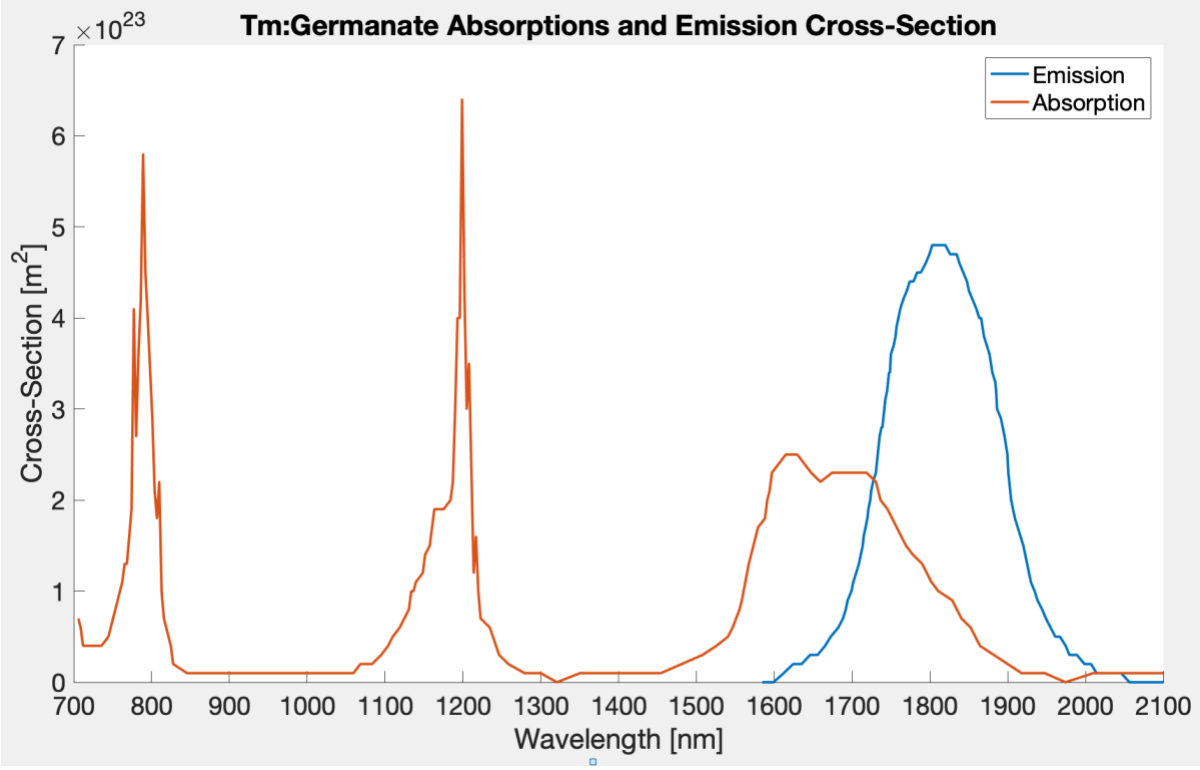

Fig.4. *Emission and absorptions cross-section spectra of Tm:germanate glass from NP Photonics.*

Chapter 2

Fiber Laser Fundamentals

Every laser system requires three fundamental components, a gain media to provide light generation and amplification, a cavity to provide optical feedback, and a pump source to provide population inversion. Fiber lasers are a subset of laser types that rely on cylindrical glass waveguides to confine the pump and laser light near an optically active core. The obvious advantage to this design is the large overlap of the pump light and gain region, which provides high gain inversion with relatively low pump powers. Other advantages include the lack of constant alignment, compact footprints, high beam quality, lower cost to manufacture, access to more obscure wavelengths [14], and relative immunity to dusty environments.

2.1 Light Amplification by Stimulated Emission of Radiation

Every laser consists of three elements, an optical cavity, a gain media, and a pumping source. A brief description of these components is given below.

2.1.1 Optical Cavity

In its simplest form, an optical cavity consists of two mirrors that are aligned such that light can be “trapped” inside for some extended period of time. The amount of time, or the number of roundtrips, light stays in the cavity is determined by the reflectivity of the mirrors. As the end goal of a laser is to emit light, one of the mirrors has less reflectivity by design. The mirror with the lower reflectivity is referred to as the output coupler. Free-space solid-state lasers typically have output couplers with reflections over 90% while fiber lasers employ output couplers with much lower reflectivity, on the order of 30%. The purpose of the cavity is to allow the emitted photons to make many roundtrips through the gain media before exiting through the output coupler. Each pass through the gain media providing amplification of the signal.

2.1.2 Gain Media

Gain media is optically active media that has a unique electronic structure that allows for population inversion. The simplest electronic structure that provides population inversion is the “three-level structure”. The three levels refer to a ground level, an excited level, and the lasing level. For most gain media, the lifetime of electrons in the excited level is so short that the decay from the excited level to the lasing level can be considered instantaneous.

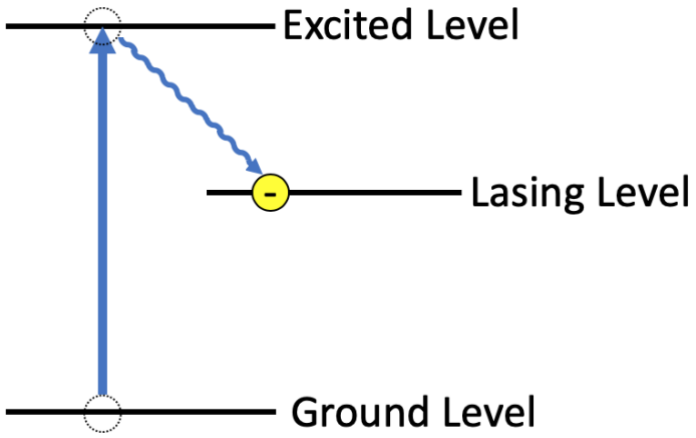

Fig. 5. *Diagram of a three-level atom.*

The other desirable trait of gain media is a long-lasing level lifetime. The longer the lasing level lifetime, the easier it is to achieve population inversion. Population inversion occurs when the ratio of ions in the excited state to the number of ions in the ground state is greater than 1.

For a given gain media at thermal equilibrium, the ratio of atoms in the excited state or ground state is given by the ratio of Boltzmann distributions,

$$\frac{N_2}{N_1} = e^{\frac{-(E_2-E_1)}{kT}} \qquad 2\text{-}1$$

where $E_2 - E_1$ is the energy difference between the excited and ground state, N_2 is the population density of the excited state, N_1 is the population density of the ground state, and k and T are the Boltzmann constant and temperature of the atoms respectively.

2.1.3 Pump Source

In order for inversion to occur, an electron from the ground state must absorb an amount of energy equal to the difference in energy between the excited level and the ground level. The excitation energy can come in the form of optical or electrical stimulation. For optical stimulation, the gain media is exposed to a photon flux where the wavelength of light is tuned to the energy difference required for excitation. Common forms of optical pumps are laser sources or flash-lamp sources. Electrical pumping can come in the form of electrical discharge, which is common in gas lasers, or electrical current, which is common in semiconductor lasers. The rate at which energy is absorbed by the ground level is equal to

$$\frac{\partial N_1}{\partial t} = -B_{12}\rho(\lambda_{12})N_1 \qquad 2\text{- }2$$

where $-B_{12}$ is the proportionality constant and $\rho(\lambda_{12})$ is the radiation energy density. The rate of absorption is also related to the instantaneous photon density, $\frac{I_\lambda}{(hv)}$, and the wavelength-specific absorption cross-section, σ_λ^α, of the gain media.

$$\frac{\partial N_1(t)}{\partial t} = -\sigma_\lambda^a \frac{I_\lambda}{(hv)} N_1(t) \qquad 2\text{- }3$$

2.1.4 Emission

Once inversion is achieved, all that is need is a spontaneous emission event to occur. Spontaneous emission, like the name implies, is the release of a photon due to the random decay

of an excited electron. In a true steady-state environment, there is no reason for an electron to unexpectedly decay from an excited state. However, in reality, fluctuations in the vacuum field provide constant perturbations to the atoms. At some point, the perturbation is just right to cause a decay event. The rate of this decay is described by the Einstein A coefficient, A_{21}, and is inversely proportional to the lifetime of the excited state, τ_{21}.

$$\frac{\partial N_2(t)}{\partial t} = -A_{21}N_2(t) = -\frac{N_2}{\tau_{21}} \qquad 2\text{-}4$$

2.1.5 Amplification

When a photon is emitted through spontaneous emission, it has a non-zero probability of interacting with a neighboring excited state atom. Like the vacuum fluctuations, an inbound photon can cause another emission event. Photon emissions occurring in this manner are referred to as stimulated emissions. For this to occur, the inbound photon must have energy similar to the energy difference of the excited state transition. Light emitted in this way has the same phase and polarization as the stimulating photon and is said to be temporally coherent. Similar to spontaneous emission, the rate of stimulated emission is given by

$$\frac{\partial N_2}{\partial t} = -B_{21}\rho(\lambda_{21})N_2 = -\sigma_\lambda^e \frac{I_\lambda}{(hv)} N_2 \qquad 2\text{-}5$$

where σ_λ^e is the emission cross-section. It is easy to see that since one photon has created two and those two will create more, coherent amplification of the original emitted photon can grow exponentially.

2.1.6 Resonance

For a laser, it is not sufficient to only have stimulated emission. Feedback of the optical signal must also occur. The end mirrors of the cavity trap the emitted light for multiple roundtrips, but due to the self-coherence, interference patterns are established. These regions of destructive and constructive interference are functions of the cavity geometry as well as the frequency of emitted light. Only light with radiation patterns that reproduce themselves on each roundtrip are considered a stable resonator mode, or eigenmode of the cavity. These cavity longitudinal modes have characteristic transverse spatial distributions, the most common being the Gaussian mode.

The number of modes that can exist in a cavity is related to the optical path-length of the cavity. For a cavity of length L, the allowed longitudinal modes are equal to an integer multiple of half the wavelength λ. The frequency spacing between adjacent modes is called the free-spectral range and is equal to the inverse round-trip time inside the cavity.

$$FSR = = \Delta\nu = \frac{c}{2nL} \qquad 2\text{- }6$$

For a given wavelength, the number of modes that can exist in a cavity is related to the ratio of the gain spectral bandwidth to the FSR.

2.1.7 Rate Equations

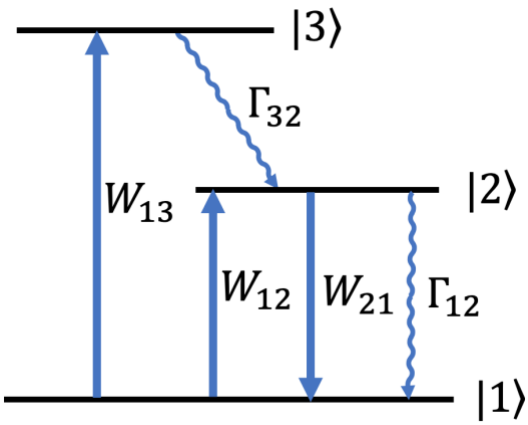

Fig. 6. *Energy level diagram of three-level atom showing rates of allowed transitions.*

For a given three level atom, the rate of population change of an energy level is equal to the sum of all the excitation and relaxation events out of and into that level,

$$\frac{dN_3}{dt} = W_{13}N_1 - \Gamma_{32}N_3 \qquad 2\text{-}7$$

$$\frac{dN_2}{dt} = W_{12}N_1 - W_{21}N_2 - \Gamma_{12}N_2 + \Gamma_{32}N_3 \qquad 2\text{-}8$$

$$\frac{dN_1}{dt} = -W_{13}N_1 - W_{12}N_1 + W_{21}N_2 - \Gamma_{12}N_2 + \Gamma_{32}N_3 \qquad 2\text{-}9$$

where N_1 is the population density of the energy level, Γ_{12} is the inverse lifetime of the energy state transition, and W_{12} is the pump rate of the relevant energy levels. W_{12} is equal to the

appropriate emission or absorption cross-section at the pump wavelength, multiplied by the pump intensity and divided by the energy of a pump photon.

$$W_{12} = \frac{\sigma_{12} I_p}{h\nu_p} \qquad 2\text{-}10$$

Typically, the excited state, state $|3\rangle$, has an decay rate fast enough compared to the other states that it can be approximated as infinite. This approximation allows us to simplify the rate equations and solve for steady state solutions by setting $\frac{dN}{dt} = 0$. The steady state solutions for a three level atom are

$$n_2 = \frac{W_{13}}{W_{13}+W_{21}+\Gamma_{21}} \qquad 2\text{-}11$$

$$n_1 = 1 - n_2 \qquad 2\text{-}12$$

where n_2 and n_1 are the normalized population densities.

2.1.8 Gain

A single signal photon emitted at L=0 within the cavity will interact with neighboring excited atoms and cause stimulated emission. As more photons are emitted into the signal mode, the signal intensity increases and gain occurs. If a traveling photon instead interacts with a photon in the ground state, loss or absorption occurs. The difference in these events is called gain.

$$g = \frac{\partial I}{\partial z} = \sigma_s^e N_2 - \sigma_s^a N_1 \qquad 2\text{-}13$$

The intensity of the original photon I_{s0} increases at a rate γ over the gain media length L as it travels through the gain media. The photon then reflects off an end mirror and travels through the gain media again, this time in the opposite direction. The photon then reflects off the other end mirror and completes a single round trip. The signal intensity after a single round trip can be described as

$$I_s = I_{s0}\kappa R_{HR} R_{OC} e^{2(g-l)L} \qquad 2\text{-}14$$

where κ and l are cavity loss factors. In this picture, gain is simply the ration of $\frac{I_s}{I_{s0}}$. While technically gain can have negative values signifying net loss, it is typically considered a positive value greater than 1. In other words, there is a threshold for gain. This threshold can be solved by rearranging equation 2-26 and setting $\frac{I_s}{I_{s0}} = 1$ and solving for g. The result is the resonator gain threshold inequality

$$g_{th} > l + \frac{1}{2L} ln\left(\frac{1}{\kappa R_{HR} R_{OC}}\right). \qquad 2\text{-}15$$

Using this threshold value to solve for the threshold state $|2\rangle$ population density N_2, yields

$$N_{2,th} > \frac{l + \frac{1}{2L} ln\left(\frac{1}{\kappa R_{HR} R_{OC}}\right) + \sigma_s^a N_t}{\sigma_s^e + \sigma_s^a}. \qquad 2\text{-}16$$

2.2 Guided Mode Propagation

Optical fiber is a dielectric waveguide that acts as a duct for electromagnetic waves. Although optical fiber can come in many geometries and refractive index profiles, for the purpose of this thesis, only cylindrically symmetric fiber with a step-index profile is considered. Optical fiber, and waveguides in general, operate on the principle of Total Internal Reflection (TIR). Core and cladding material is chosen such that the core index n_c is higher than the cladding index n_d. The degree to which the core and cladding refractive indices differ determines the level of confinement of the propagating light. Typically, the difference in index between the core and the cladding is small and is represented by

$$\Delta \equiv \frac{n_c^2 - n_d^2}{2n_c^2} \approx \frac{n_c - n_d}{n_c} \ll 1 \qquad 2\text{-}17$$

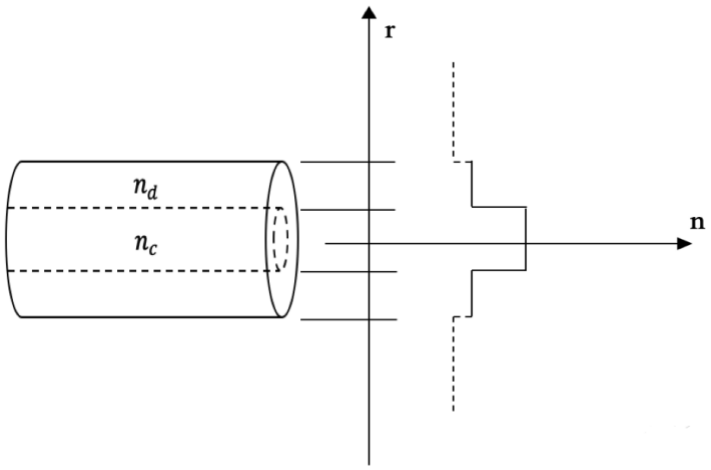

Fig. 7. *Radial index profile of step-index fiber.*

2.2.1 Total Internal Reflection

Total Internal Reflection (TIR) describes a unique case when an incident ray of light is completely reflected at the interface of two transparent media. The required angle of incidence can be easily determined by Snell's Law by setting $\theta_2 = 90°$.

$$n_1 \, sin(\theta_1) = n_2 \, sin(\theta_2) \quad \rightarrow \quad \theta_1 = sin^{-1}(\frac{n_2}{n_1}) \qquad 2\text{-}18$$

Under these circumstances, θ_1 is referred to as the critical angle or θ_c. All light rays that have incident angles larger than the critical angle will be completely reflected and continue to rattle down the cylindrical waveguide. As the difference in index between the core and cladding increases, the critical angle decreases. This results in a larger set of incident angles that will still

satisfy TIR. θ_c also determines the numerical aperture of the waveguide. The numerical aperture is a description of the acceptance cone that defines the largest angle a ray can be launched into a fiber a still satisfy TIR. As this is a time reversible phenomenon, the NA also describes the divergence angle of light emitted from a fiber.

$$NA = nsin(\theta_{max}) = \sqrt{{n_c}^2 - {n_d}^2} \approx n_c\sqrt{2\Delta} \qquad 2\text{-}19$$

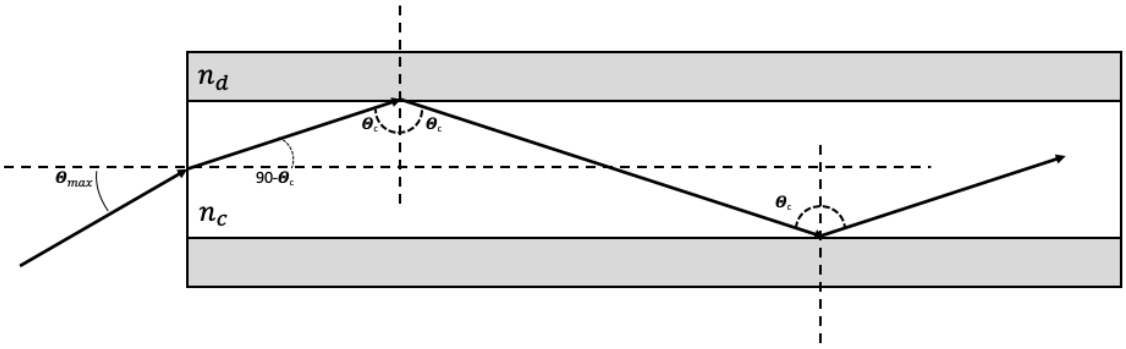

Fig. 8. *Diagram of TIR condition in step-index fiber.*

2.2.2 Guided Modes

In order to solve for the electric field inside the fiber, one can use Maxwell's equations and the appropriate boundary conditions governed by the cylindrical geometry of the fiber. Due to the multiple reflections experienced by the guided field, a self-consistency condition can be applied such that the field after two consecutive reflections reproduces itself. In other words, the phase shift before and after two reflections must be zero or a multiple of 2π. Waves that satisfy

this condition have fields that maintain the same transverse profile at all points along the fiber axis. Such fields are referred to as modes of the waveguide.

These modes represent special solutions to Maxwell's equations. Each mode has a definite propagation constant, a characteristic transverse field distribution, and can be polarized in two completely independent states [1]. The conditions under which a wave satisfies this self-consistency condition is determined by the geometry of the waveguide, the wavelength of the transmitted light, and the incident angle of a wave-front.

While Maxwell's equations provide exact solutions for field distributions in a dielectric cylinder [15], this method is excessively complicated [16]. For practical purposes, much simpler methods can be used. For a step-index fiber, the time-independent fields can be solved exactly by the Helmholtz equation [1].

$$\nabla^2 U + n^2(r) k_0 U = 0 \qquad \textit{2- 20}$$

where $k_0 = \frac{2\pi}{\lambda_0}$ and $n(r) = \begin{cases} n_c \; if \; r < r_{core} \\ n_d \quad else \end{cases}$.

Rewritten in cylindrical coordinates

$$\frac{\partial^2 U}{\partial r^2} + \frac{1}{r}\frac{\partial U}{\partial r} - \frac{1}{r^2}\frac{\partial^2 U}{\partial \phi^2} + \frac{\partial^2 U}{\partial z^2} + n^2 {k_0}^2 U = 0. \qquad \textit{2- 21}$$

Here, $U = U(r, \phi, z)$ represents the field inside the optical fiber. Since this field travels in the z-direction with propagation constant β, we can write the z-component of U in the form $e^{-i\beta z}$. Similarly, the periodic nature of the angular component can be written as $e^{-il\phi}$, where l is an integer. Therefore, the general solution of the field can be written as

$$U(r, \phi, z) = u(r)e^{-i\beta z}e^{-il\phi}. \qquad 2\text{-}22$$

Plugging this into equation *2-10* yields the ordinary differential equation

$$\frac{\partial^2 u}{\partial r^2} + \frac{1}{r}\frac{\partial u}{\partial r} + \left(n^2(r){k_0}^2\beta^2 - \frac{l^2}{r^2}\right)u = 0. \qquad 2\text{-}23$$

Here, the propagation constant β is the rate of phase change as the field propagates along $\hat{z}$.

$$\beta \equiv k_z = kcos\theta \qquad 2\text{-}24$$

Due to the modal nature of waveguide propagation, the propagation constant can be quantized with each mode having its own distinct value.

$$\beta_m = n_c k_o = k_o cos\theta_m. \qquad 2\text{-}25$$

Since $cos\theta_m$ has values between 1 and $cos\theta_c = \frac{n_d}{n_c}$, β_m has values from $n_d k_o$ to $n_c k_o$ [1]. That is to say that the propagation constant of a wave must be greater than the wavenumber of the cladding but smaller than the wavenumber of the core in order for the wave to be guided [1]. With this result in mind, it is useful to define

$$k_T^2 = n_c^2 k_o^2 - \beta^2 \qquad \textit{2- 26}$$

and

$$\gamma_T^2 = \beta^2 - n_d^2 k_o^2. \qquad \textit{2- 27}$$

Substituting these into equation *2-12* we get

$$\frac{\partial^2 u}{\partial r^2} + \frac{1}{r}\frac{\partial u}{\partial r} + \left(k_T^2 - \frac{l^2}{r^2}\right)u = 0, \quad r < a\ (core) \qquad \textit{2- 28}$$

$$\frac{\partial^2 u}{\partial r^2} + \frac{1}{r}\frac{\partial u}{\partial r} - \left(\gamma_T^2 + \frac{l^2}{r^2}\right)u = 0, \quad r > a\ (cladding). \qquad \textit{2- 29}$$

Equations *2-17* and *2-18* have solutions belonging to the family of Bessel functions. The type of Bessel function is radially dependent since the solution for inside the core and inside the cladding is different. Excluding solutions with discontinuities, the bounded solutions are

$$u(r) \propto \begin{cases} J_l(k_T r), & r < a\ (core) \\ K_l(\gamma_T r), & r > a\ (cladding) \end{cases} \qquad \textit{2- 30}$$

J_l and K_l are the l^{th} order Bessel functions of the first and second kind respectively.

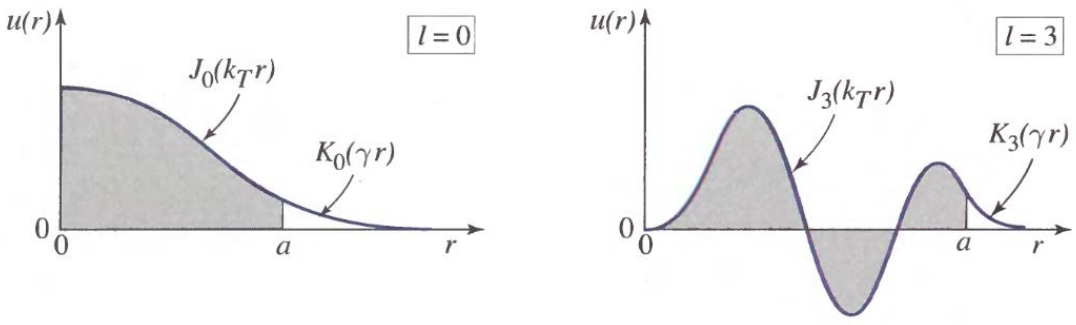

***Fig.9**. Radial distributions of $u(r)$ for l=0 and l=3 [1].*

For single-mode fiber, only the *l=0* mode is allowed to exist.

Chapter 3

Single-Frequency Fiber Lasers

3.1 Motivation

A single-frequency laser is a laser that operates in a single cavity mode and thus emits light with a very narrow spectral linewidth and low phase-noise. These qualities make single-frequency lasers useful in applications that require very long temporal coherence lengths such as distributed acoustic sensing (DAS), light detection and ranging (LiDAR), nonlinear frequency conversion, atomic cooling, coherent beam combining, and many others [17]. Low relative intensity noise (RIN) is also a characteristic of single-frequency lasers as there are no other modes to beat against. Low RIN makes single-frequency lasers also useful in RF Photonics and optical data storage, where amplitude fluctuations can disrupt data transfers.

3.2 Design

As described in chapter 2.2.6, the number of modes supported in a laser cavity can be approximated as the ratio of the gain spectral bandwidth and the cavity's free spectral range (FSR). This leads us to the most obvious approach to achieving single-mode operation, reducing cavity length. As the cavity gets smaller, the frequency spacing between adjacent longitudinal

modes increases. If the spacing gets large enough, the adjacent modes are pushed to the tails of the gain bandwidth and below the lasing threshold.

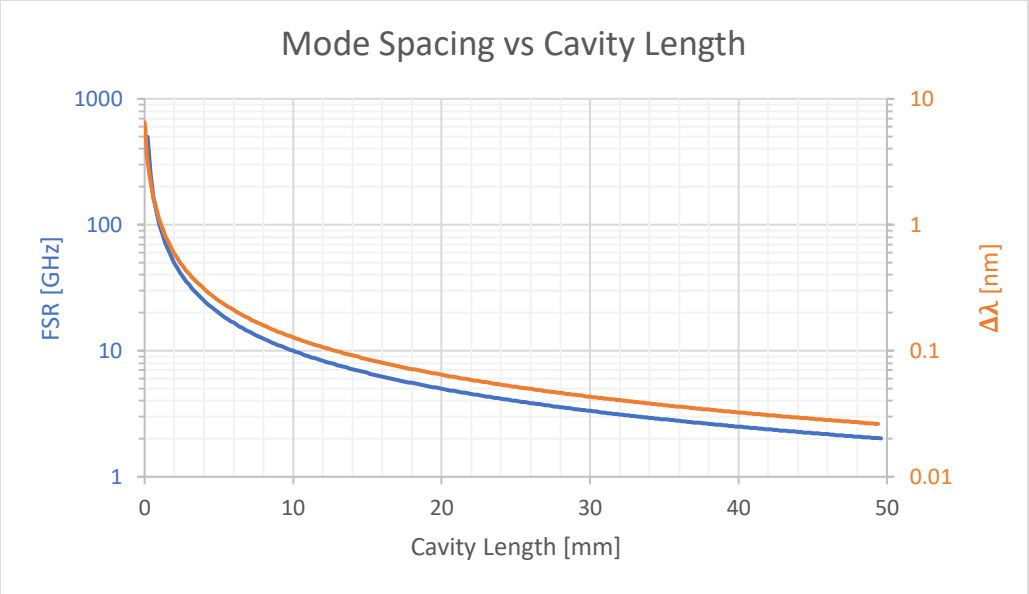

Fig. 10. *Cavity mode spacing as a function of the cavity length.*

While this approach is rather simple, as Figure 10 shows, the drawback is that the cavity becomes so small that it is now hard to achieve significant output powers. This can be an issue in single-frequency semiconductor lasers, where the cavity output power is on the order of 5mW [18].

In order to get around this issue, an additional component can be added to the cavity to restrict the allowed lasing bandwidth and allow for the FSR to get smaller while still maintaining a single-mode within the spectral window. In semiconductor lasers, this may be in the form of wavelength-selective high-reflection (HR) and anti-reflection (AR) coatings on the end facets.

Fiber-based cavities, on the other hand, are able to utilize narrowband FBGs to achieve spectral restriction. Narrowband FBGs are capable of achieving reflection bandwidths of <0.05nm. Furthermore, all fiber cavities allow for polarized output directly from the cavity. If the output coupler (OC) FBG is written on polarization-maintaining (PM) fiber, the difference in index between the fast and slow axes causes the two polarization modes to be separated in wavelength by an amount that can easily be larger than the reflection bandwidth of the HR. This forces the cavity to operate in a particular polarization mode since the other mode is not allowed to reflect by the end mirrors.

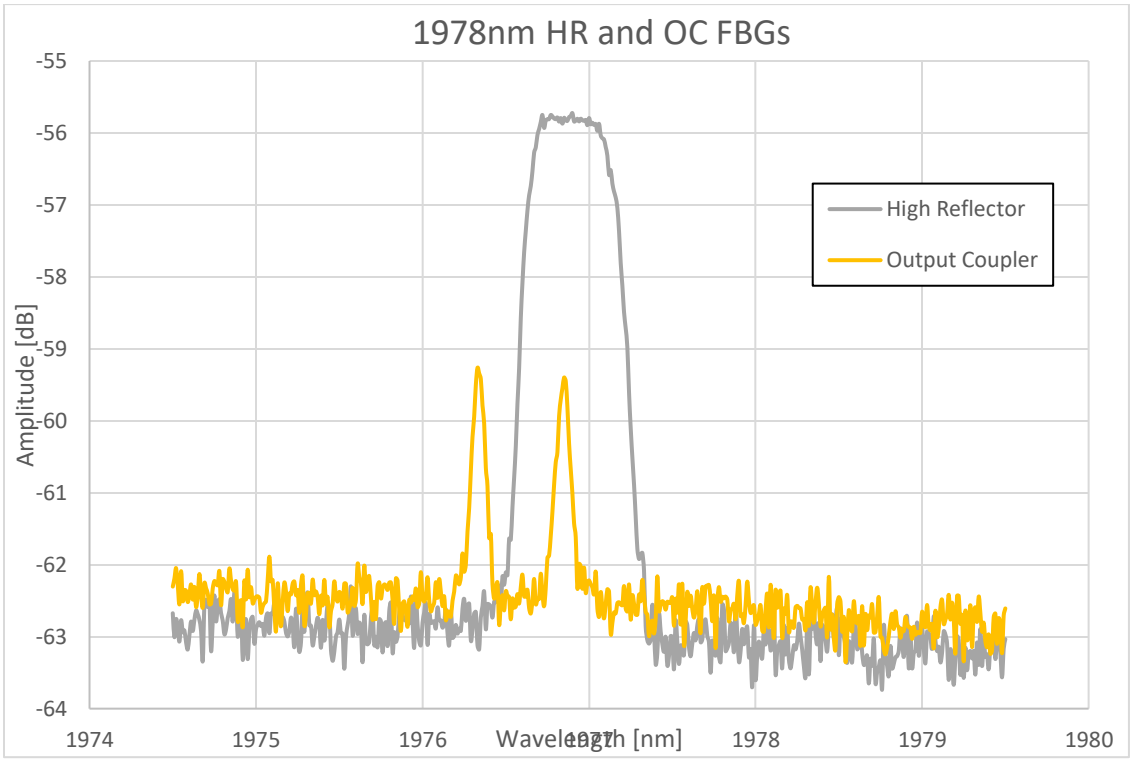

Fig. 11. *Reflection spectra of HR and OC FBGs.*

3.3 Experimental Setup

In order to overcome the issue of low gain in small cavity volumes, a very highly doped germanate glass from NP Photonics was chosen. This fiber exhibits a Tm+ weight concentration percentage of 4%, significantly larger than commercial Tm+ doped silica fiber.

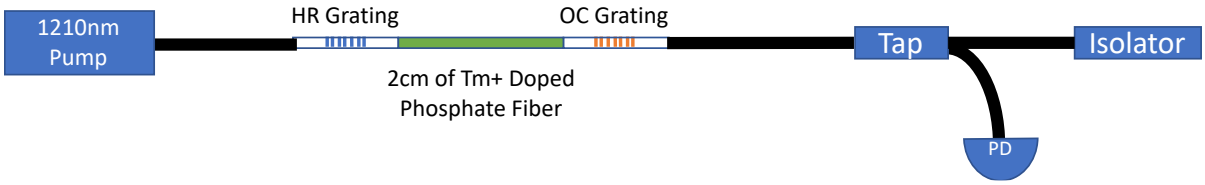

Fig.12. *Diagram of single-frequency fiber laser including 1210nm pump diode, laser cavity, fiber tap, power monitoring photodiode, and output isolator.*

The single-frequency laser configuration, as depicted in Figure 12, consists of a simple distributed Bragg Reflector (DBR) style resonator pumped by a single 500mW 1210nm FBG stabilized diode. The cavity was fabricated by cleaving a high-reflecting (HR) FBG and a partial reflecting (PR) FBG very close to the grating region of the fiber. These FBGs were then carefully spliced to ~2cm of NP Photonics' thulium-doped germanate gain fiber. A mechanically strong fusion splice was achieved via a Vytran fusion splicer. The reflection spectra of both the HR and PR FBGs are depicted in Figure 11.

High concentration commercial Tm:silica fiber was also tested under these conditions to verify that NP Photonics' fiber was necessary for this application. No other commercial fiber was able to provide gain with just 2cm of fiber. Longer lengths of commercial fiber were then tested to compare gain.

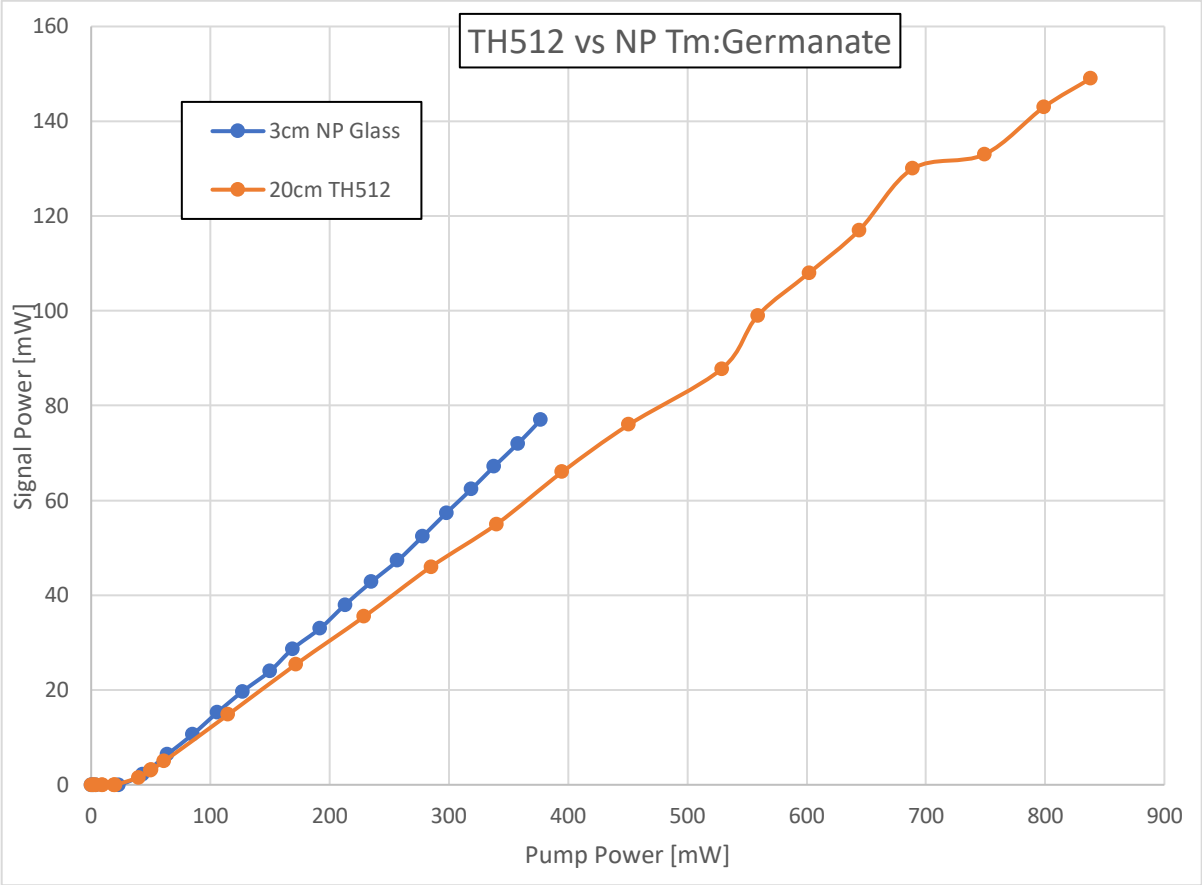

Fig. 13. *Laser performance of commercial Tm:silica fiber and NP Tm:germanate fiber.*

3.4 Gain Media Characterization

In order to determine the best pump wavelength for a packaged device, the output signal power as a function of pump power was measured at 793nm, 1210nm, and 1573nm. Each wavelength has their pros and cons, outlined below.

793nm

Light at 793nm has the strongest absorption and therefore provides the highest slope efficiency. 793nm also has the advantage of >1 quantum efficiency due to the cross-relaxation phenomenon. Cross-relaxation occurs when neighboring Tm+ ions are close enough to interact with each other via electric dipole-dipole interactions. When this occurs, a single absorbed photon can result in two photons decaying into the upper lasing state. This effect results in a quantum efficiency greater than one [11]. Normally, this would mean that the efficiency of a laser pumped at 793nm would be less affected by temperature. However, because the cross-relaxation phenomenon is mediated by phonons, the process is actually very temperature-dependent. During my testing, it was determined that the concentration of Tm+ ions may have been too high. Such a high concentration, while giving access to cross-relaxation, also resulted in large amounts of non-radiative decay. This loss of excited level electrons through ion-ion collisions made the fiber chain hot and reduced the efficiency of the cross-relaxation process.

High temperature sensitivity could be seen in variations of output power for uncooled and cooled samples (Figure 14). Occasionally, lack of optical to optical efficiency can be compensated by pumping the system harder. However, since the goal of this research was to develop a production-quality laser module, only butterfly-style laser diodes were considered and high power single-mode diodes at 793nm are not available commercially.

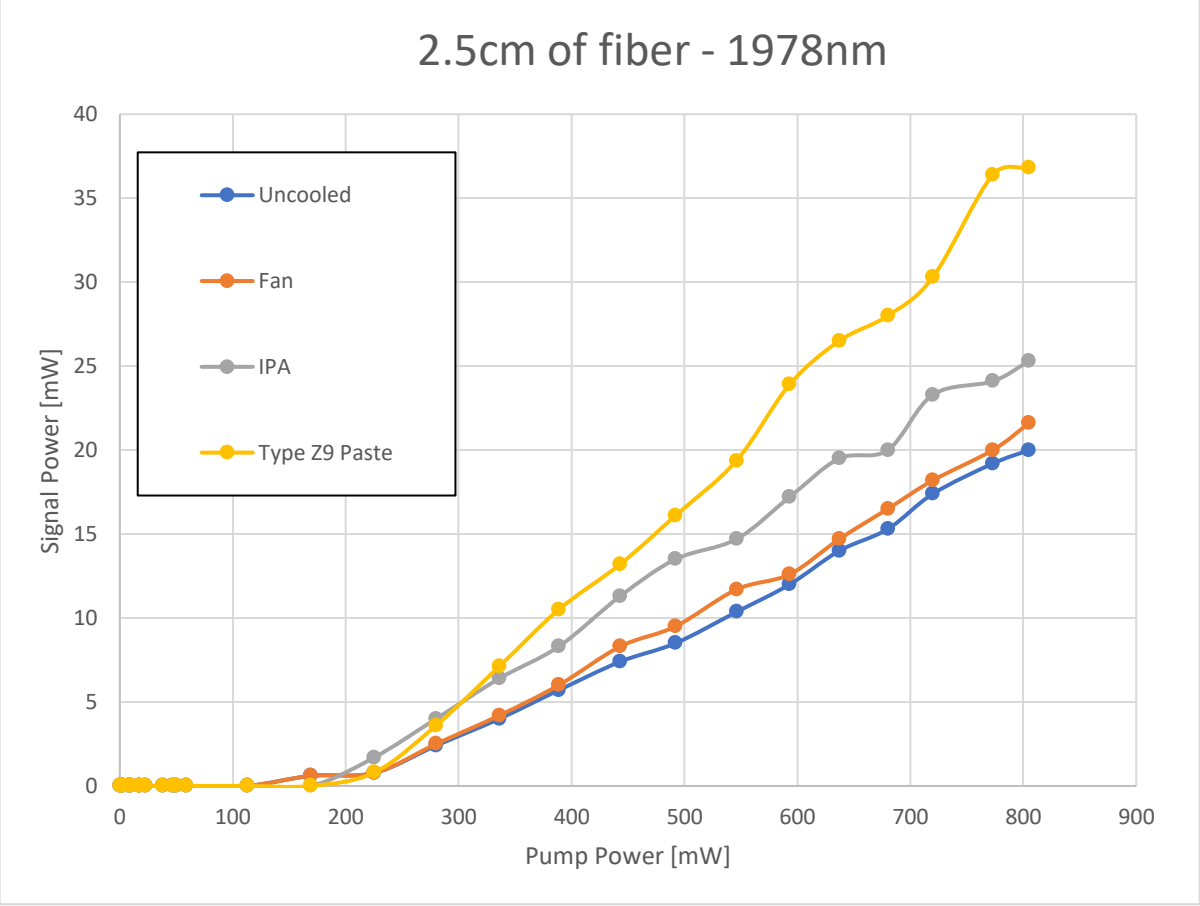

Fig.14. *Comparison of thermal management effect on laser performance.*

1210nm

1210nm was also an attractive pump wavelength due to the commercial availability of high power single-mode pump diodes. As seen in Figure 15, the increased pump power availability was able to outweigh the benefits of pumping with a 793nm diode.

1573nm

1573nm is a very common fiber laser source and therefore quite easy to get relatively high power (>1W). Within my package constraints, a 1573nm source could be generated by using two 980nm single-mode pump diodes to pump a fiber cavity of Erbium-doped Silica fiber. The output of this laser could then be used to pump the Tm+ doped single-frequency cavity. Data was taken to see the optical to optical efficiency of pumping at 1573nm. This approach was not fully considered as the components required were too expensive for the final design.

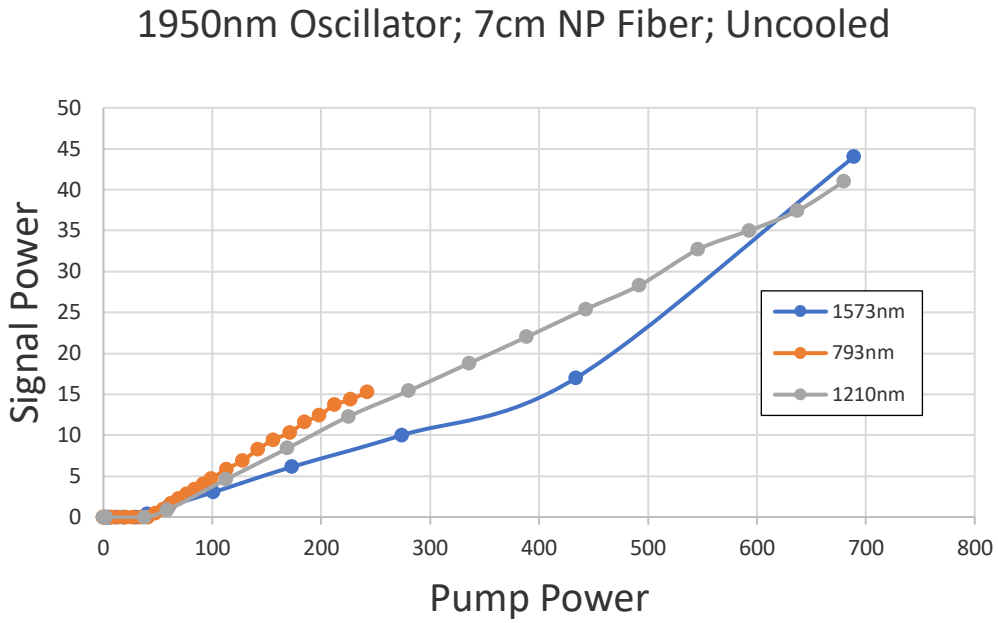

Fig. 15. *Effect of pump wavelength on laser output using NP Fiber.*

3.5 Assembly and Characterization

In order to achieve a short cavity, the two FBGs were cleaved very close to the start of the grating region and spliced to a small section of NP Tm+ gain fiber. The cavity was then placed in a ceramic block to provide thermal stability in the cavity region. A diagram of the laser design can be seen in Figure 12. For this particular device, a signal wavelength of 1978nm was needed. Fiber Bragg gratings resonant to this wavelength were purchased from OE Land.

Several lengths of gain fiber we tested in order to determine the ideal cavity length. Shorter lengths would assist single transverse mode operation but would restrict the available

output power. Ultimately, 20mm of gain fiber was chosen as it provided satisfactory output power and broader mode spacing.

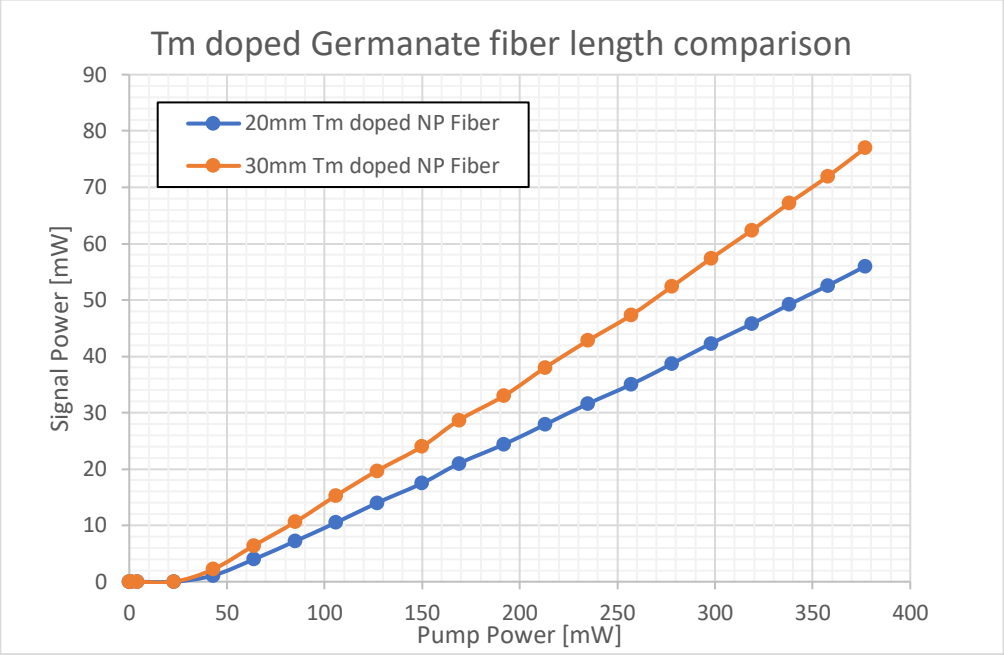

Fig.16. *Laser output as a function of gain media length.*

The constant temperature of the cavity translates to frequency stability and is critical for applications that require low phase noise and cannot tolerate frequency drift. Embedded in the ceramic oven is a thermistor for temperature monitoring and a small piezo. The piezo, which is affixed to one end of the cavity, allows for small, accurate stretching of the cavity. The piezo also provides the ability to achieve small, quick shifts in output wavelength and can be used to avoid the presence of second modes. The presence of a secondary transverse mode is detected with a fast photodiode at the output of a small evanescent tap. When two modes are simultaneously lasing, their difference in cavity roundtrip time will result in a beat mode. This

beat mode is in the MHz domain and can be detected with a fast enough detector. A threshold voltage on the photodiode can then be set to trigger the piezo to shift to a predetermined value. These values are established during a calibration step where the cavity temperature is scanned over the full range while monitoring second mode events. For additional environmental isolation, steps were taken to dampen any mechanical vibrations that may couple into the cavity.

Wavelength tunability was achieved by controlling the temperature of the FBG pair. As the fiber stretches and contracts with temperature, the shape of the FBG grating structure changes and thus the wavelength it is resonant with shifts accordingly. Controlling the cavity temperature via heater allows one to tune to output wavelength of the cavity over ~0.5nm. A PID loop ensures the temperature of the cavity is kept at the desired set point. Although the cavity is extremely stable in constant current mode, an additional power monitoring diode can be used to update pump diode current to reduce output power noise if necessary.

Due to the difficulty of splicing dissimilar glass, there can be high variability in optical efficiency from unpredictable splice loss. Slope efficiencies ranged from 15% - 6% with a single outlier at >20%. Based on this, it is reasonable to assume better efficiency could more regularly be achieved with an optimized splice routine. Achieving a consistent splice recipe is critical since additional attempts increase the chance of damaging the nearby FBGs.

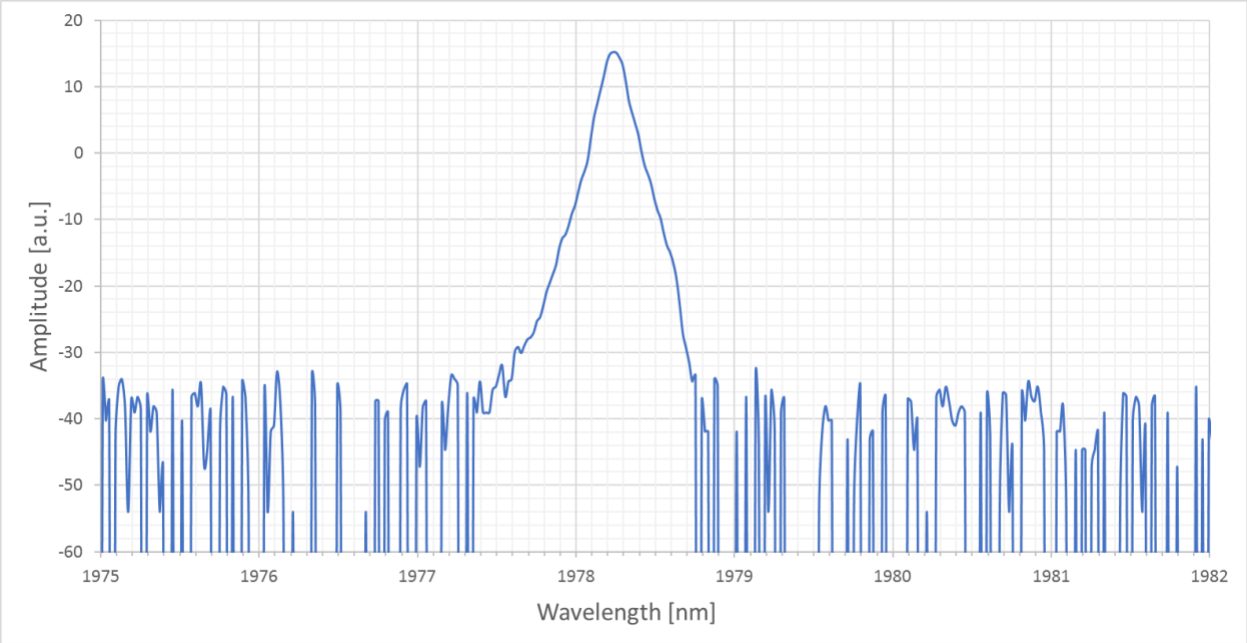

Fig.17. *Emission spectra of 1978nm laser.*

Chapter 4

Thulium:Germanate Slab Amplifier

4.1 Motivation

Many commercial and military LiDAR applications require single-frequency laser sources with millijoule or more pulse energies [3,4]. Achieving pulse energies above several millijoules in fiber-based systems proves difficult due to nonlinear effects like Stimulated Brillouin Scattering (SBS), Self-Phase Modulation (SPM), and Stimulated Raman Scattering (SRS) [19]. One approach to reaching higher energies in all fiber systems is to utilize large mode area (LMA) fiber, which reduces optical power density while maintaining single-frequency operation. However, weakly guiding fiber is more susceptible to modal instability, especially at high powers [20].

Recently, free-space slab style amplifiers have been used to scale to higher energies while avoiding unnecessary travel in non-linear media [21]. Slab amplifiers are similar to rod architectures, yet the rectangular shape provides convenient cooling surfaces and allows for bi-directional pumping schemes. While slab amplifiers have historically utilized crystalline host media, recent advances in glass technology show potential for cheaper solutions.

4.2 Experimental set-up

For this research, high concentration thulium-doped Germanate glass was used as gain media. The glass was cut and polished into a 20mm x 10mm rectangle with various thickness ranging from 300μm to 1mm. As in all high-power amplifiers, cooling of the gain media to some constant temperature is critical. Here, this was achieved via water-cooled copper heatsinks placed on the top and bottom of the slab. Indium foil was also used at the copper glass interface in order to fill any surface defects and minimize hot spots. A diagram of the heatsink can be seen in Figure 18.

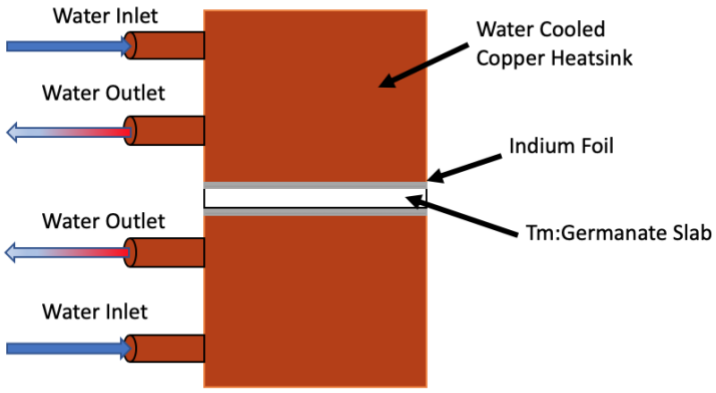

Fig.18. *Diagram of glass slab cooled by water-cooled copper heatsink.*

CVD diamond was also investigated as a possible thermal interface material. The large thermal conductivity of diamond (>1000$Wm^{-1}K^{-1}$) will act as a heat spreader and pull heat out of the glass slab much more efficiently than just copper heatsink. 10mm x 10mm x 0.5mm

polycrystalline CVD diamond wafers were purchased from element6TM and bonded to Tm:germanate slabs with similar dimensions via a titanium-gold eutectic solder.

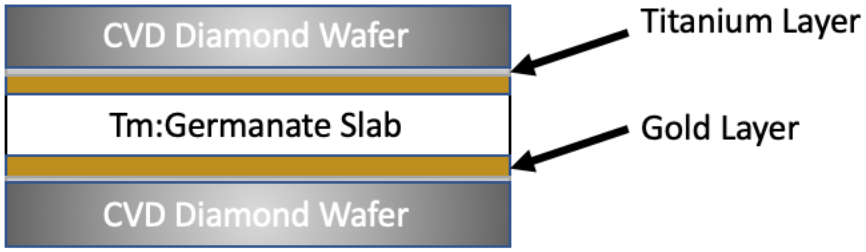

Fig.19. *Diagram of glass slab bonded to CVD diamond wafer.*

Optical pumping of the amplifier was achieved via six 50W 793nm fiber-coupled semiconductor diodes. Each diode was combined into a single fiber channel with a 7x1 pump combiner. A short focal length objective lens was used to collimate the output of the multimode pump. The beam diameter after the collimating lens was ~1mm. The pump beam was then expanded to 20mm, matching the width of the slab, by propagating the beam through a 20 to 1 telescope. Finally, a pair of cylindrical lenses were used to provide slight focusing in the horizontal plane and significantly sharper focusing in the vertical plane. Even though the pump light was highly multimode, optics were chosen to achieve a vertical plane Rayleigh range longer than the length of the slab.

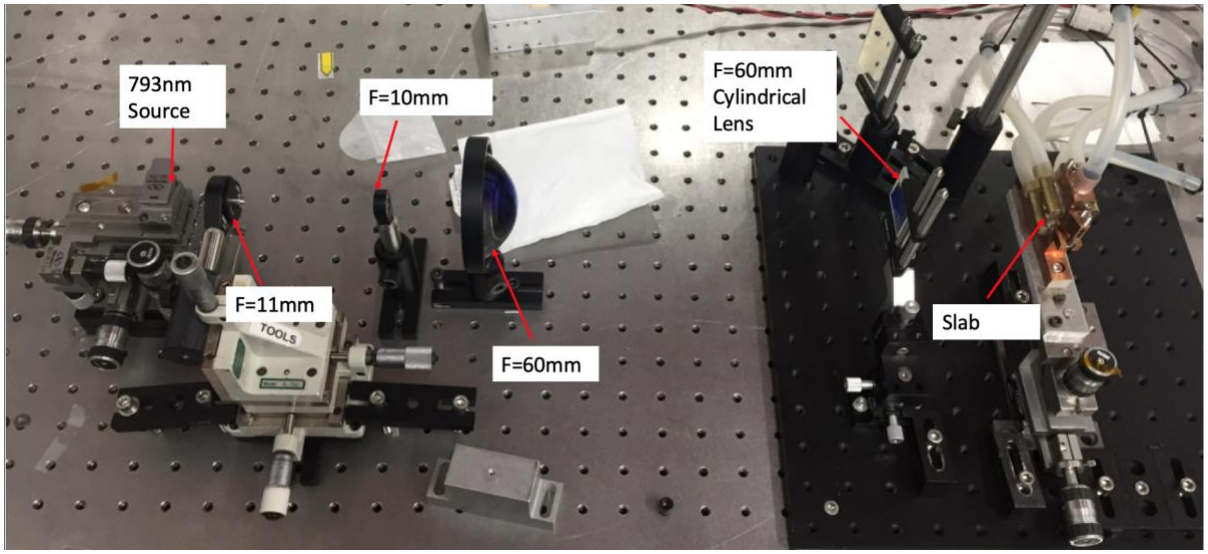

Fig.20. *Image of slab pump optics.*

The pump optics were modeled in Zemax to confirm their design and to understand the field's cross-sectional irradiance pattern at the slab surface.

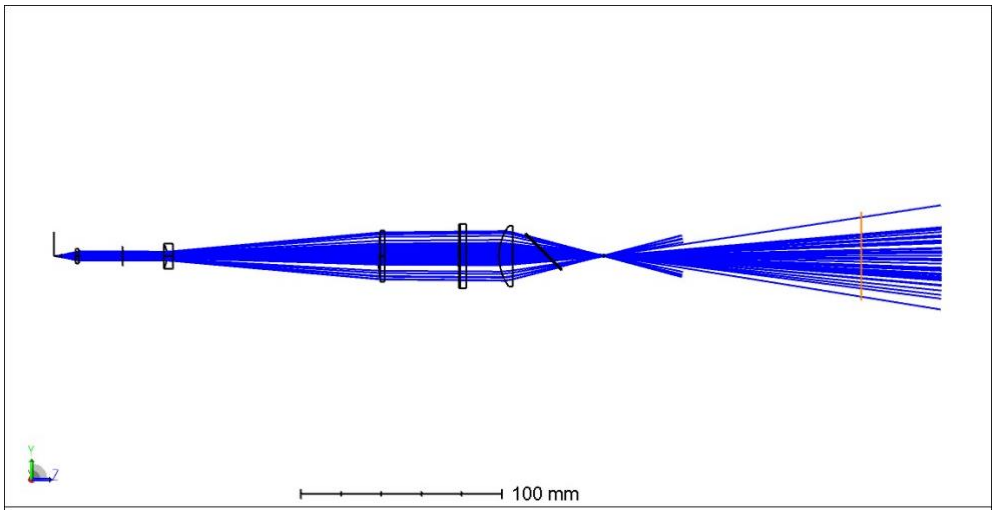

Fig.21*. Zemax model of pump optics.*

Even though the doping concentration of the glass was quite high (4%), it was expected that single-pass gain would be low. To combat this, the signal beam was designed to have multiple passes through the slab. The angle of the reflected signal beam was made large enough so that the signal would see an “un-seeded” section of gain media. Cylindrical focusing end mirrors were used to allow the signal beam to freely expand in the horizontal direction while maintaining the proper beam height within the slab. The combination of the pump and signal beam was accomplished by 0° dichroic mirrors. The optical design was also confirmed by Zemax simulation [Fig. 21]. However, due to limitations in performance, implementation of the zig-zag signal propagation scheme was never realized.

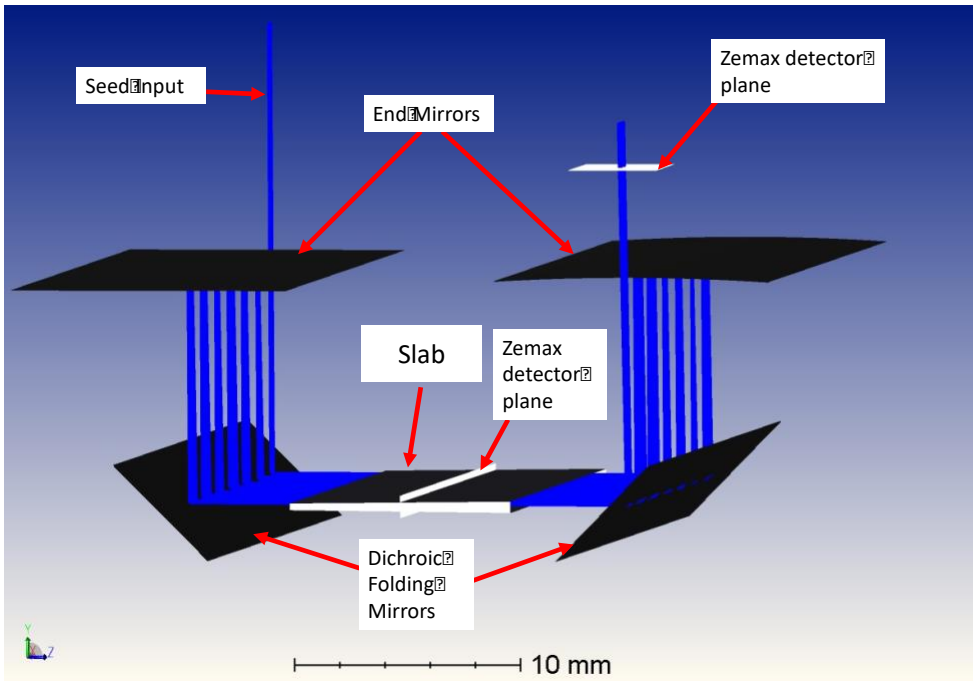

Fig.22. *3D model of signal beam optics.*

4.3 Performance

The biggest hurdle for glass-based slab amplifiers is the poor thermal conductivity of the Tm:germanate glass (0.6 $Wm^{-1}K^{-1}$). As mentioned in Chapter 1.3, the gain efficiency of thulium-doped germanate is very sensitive to temperature thus it is critical to cool the slab. While the heatsink was able to successfully cool the top and bottom surface, a steep temperature gradient was created due to the elevated temperature near the center of the slab. As pump power increased towards the gain threshold, the temperature gradient would become too steep and the glass would crack.

Another drawback to this design is the large pumping surface area. This leads to a scenario where the integrated pump power can be quite high, 600W, while the power density is low, 6kW/cm^2 for a 0.5mm thick slab. Both the pump power and thermal gradient issues can be addressed by reducing the slab thickness, yet handling and optical alignment can be difficult. Additionally, double-sided pumping can be utilized to increase inversion across the slab while distributing the thermal load across two surfaces. Measured survivability of the slab for different thicknesses and pumping schemes can be seen in figure 23.

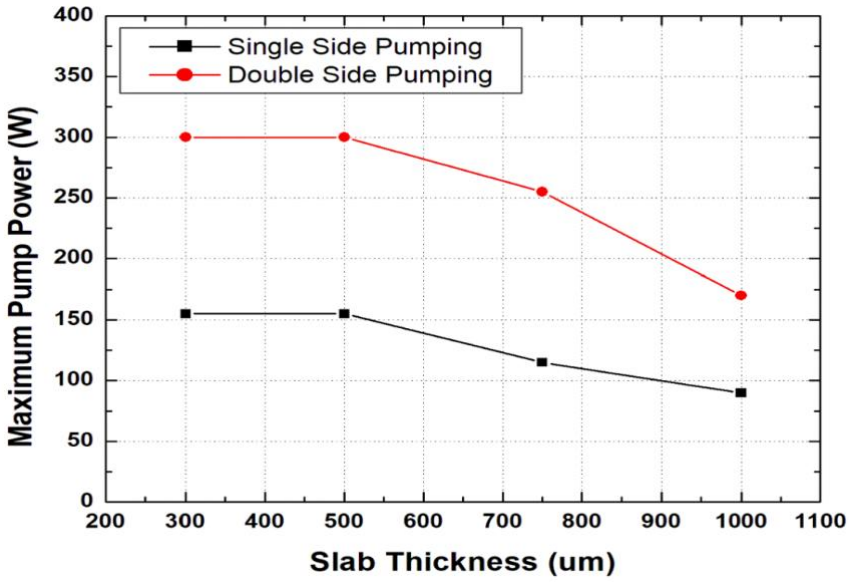

Fig. 23. *Slab failure points due to thermal effects for several slab thickness for both single-side and bidirectional pumping.*

4.4 Modeling

Gain modeling for the slab amplifier was performed in MATLAB to better understand how far away we were from the gain threshold. Many different parameters were varied to explore the systems performance landscape. All simulations assume a 1mm thick slab, a uniform 20mm x 1mm pump profile, and a CW signal power of 1W. Using the relevant absorption coefficient, absorbed pump light at every linear position in the slab was calculated and then used to determine pump rate as a function of slab position. Excited level population was then calculated using equations 2-11 and 2-12.

As mentioned above, bidirectional pumping is favorable for thermal distribution inside the glass slab. As expected, it also helps with population inversion across the slab. The effect of the pumping scheme on population inversion can be seen in Figure 24.

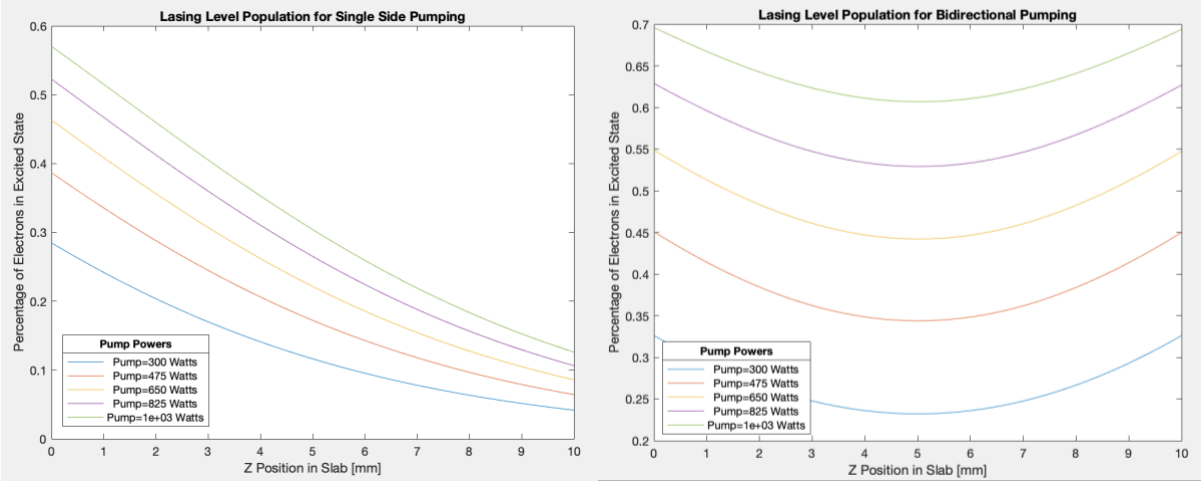

Fig. 24. *A plot of excited state normalized population as a function of position in the slab for single sided pumping(left) and bidirectional pumping (right). Pump powers are listed per side.*

The increased inversion results in more ions available to contribute to gain, as seen in Figure 25. Roundtrip gain was calculated by using equation 2-13 and propagating a signal in a stepwise manner through the slab in the forward direction and then in the backward direction. This process was repeated for every roundtrip.

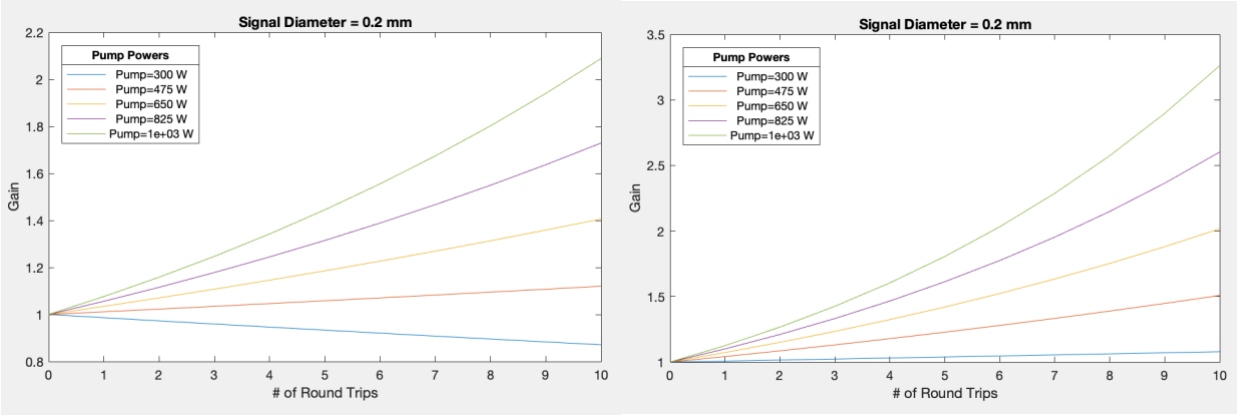

Fig. 25. *Accumulated gain versus number of round trips for single sided pumping(left) and bidirectional pumping (right). Pump powers are listed per side.*

Since the goal of the slab amplifier is to amplify high-intensity signal beams, it is important to investigate how gain changes with varying signal intensity. Assuming bidirectional pumping, the simulation results below show the influence of changing the effective signal diameter. Increasing the signal diameter decreases the signal intensity while maintaining integrated power. As the signal intensity decreases, it moves further away from the saturation intensity, leading to more gain. A larger beam also covers more of the gain media and therefore will be interacting with more excited ions.

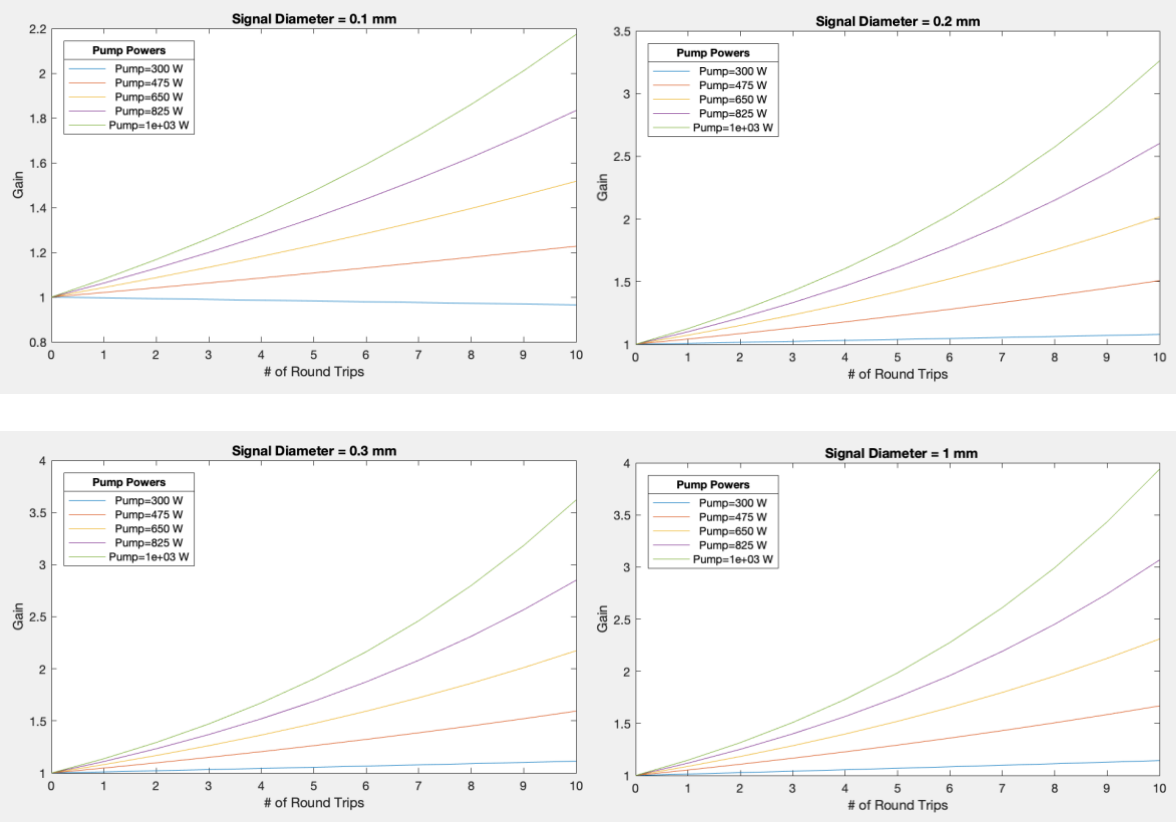

Fig. 26. *Effect of signal beam diameter on gain for bidirectional pumping. Pump powers are listed per side.*

In conclusion, from similar research [21] it is clear that slab amplifiers are capable of being a critical tool in high energy laser systems. However, glass-based solutions require significant research before they can compete with crystal gain media. Lowering doping concentrations and reducing the thickness of the slab should help drastically with the thermal issues presented here. Additionally, simulations demonstrate significant gain can be achieved with large numbers of passes through the gain region. Changing the slab dimensions to facilitate more passes could prove very beneficial.

APPENDIX A – Slab Amplifier Code

```
clear;
clc;

%% Physical Constants
h = 6.626*10^(-34);        %Planck constant; unit: J*s
c=2.9*10^8;               %light speed; unit: m/s

%% Thulium Characteristics
Ntot = 5.3E26; % [m^-3] Number Density
A20 = 5E-3; % IN SILICA 5ms upperstate lifetime

%% Slab
SlabArea = (20E-3)*1E-3; %[m^2]
SlabLength = [10]; %Slab length 10mm
Slablength = SlabLength*10^(-3);
figureCell = cellstr(num2str(SlabLength','Slab Length = %.3g mm'));
for ii = 1:length(Slablength)
L = linspace(0,Slablength(ii),1000); %Discretizing Length

%% Pump
TotalPump = linspace(300,1000,5);%[W]
Inten  = [5,10,15,20,25,30];
PumpArea = SlabArea;
Ip_in = TotalPump/PumpArea;
lambda_P=793*10^(-9);   %pump wavelength; 793nm; unit: m
nu_p=c/lambda_P;   %Pump Frequency
overlap = 1;
%% Signal
lambda_S=1.96*10^(-6); %signal wavelength; 1.920 um; unit: m
nu_s=c/lambda_S;         %laser frequency;
SignalDiameter = [100,200,300,1000,3000,5000]; %[um]
SignalArea = pi*(0.5*SignalDiameter*10.^(-6)).^2; %[m^2]
Ps_in =1; %Watt
Is_in = Ps_in./SignalArea;

%Seed/Pump/Gain Calculated values
[cross03,cross30]=cross(lambda_P); %Pump abs and emm cross sections
[cross02,cross20]=cross(lambda_S); %Signal abs and emm cross sections
alpha = Ntot*cross03; %[m^-1] Absorption Coefficient
Absorption = 1-exp(-alpha*L);  %Absorption
Esat = SignalArea*h*nu_s/(cross20-cross02); % [J] Saturation Energy
Psat = Esat/A20; %[Watts]
Isat = Psat./SignalArea; % [Watts/m^2]
```

```
%% Preallocation
Ip = zeros(length(L),length(Ip_in));
Is = zeros(length(L),length(Is_in));
W03 = zeros(length(L),length(Ip_in),length(Is_in));
W02 = zeros(length(L),length(Ip_in),length(Is_in));
W20 = zeros(length(L),length(Ip_in),length(Is_in));
n3 = zeros(length(L),length(Ip_in),length(Is_in));
n2 = zeros(length(L),length(Ip_in),length(Is_in));
n0 = zeros(length(L),length(Ip_in),length(Is_in));
g_ss = zeros(length(L),length(Ip_in),length(Is_in));
g = zeros(length(L),length(Ip_in),length(Is_in));
%G = zeros(length(L),length(Ip_in),length(Is_in));
%Inversion = zeros(length(L),length(Ip_in),length(Is_in));
Ps = zeros(length(L),length(Ip_in),length(Is_in));
PsBack = zeros(length(L),length(Ip_in),length(Is_in));

%% Initial Conditions
n0(1,:) = 1; %Normalized pop all in ground state at t=0
Ip(1,:) = Ip_in; %W/m^2
Is(1,:) = Is_in;
Is = repmat(Is,1,1,length(Ip_in));
Is = permute(Is,[1,3,2]);

%% Pump Absorption
for i = 1:length(Ip_in)
    for j = 1:length(L)
        Ip(j,i) = Ip(1,i)*exp(-alpha*L(j));
    end
end
IpBack = flip(Ip);
AsymPumpRatio = 1;
Ip= Ip+IpBack+AsymPumpRatio*IpBack;
Ip= repmat(Ip,1,1,length(Is_in));



%% Pump Rate and Population Levels
%%Forward
for k = 1:length(Is_in)
    for j = 1:length(Ip_in)
        for i = 1:length(L)
            W03(i,j,k) = cross03*Ip(i,j,k)/(h*nu_p);
            W02(i,j,k) = cross02*Is(i,j,k)/(h*nu_s); % 1->2 pump rate
            W20(i,j,k) = cross20*Is(i,j,k)/(h*nu_s); % 2->1 pump rate
            n2(i,j,k) = W03(i,j,k)/(W03(i,j,k)+W20(i,j,k)+1/A20);
            n0 (i,j,k) = 1-n2(i,j,k);
```

```
            g_ss(i,j,k) = overlap*Ntot*(cross20*n2(i,j,k)-
cross02*n0(i,j,k));
            delZ = L(2)-L(1);
            g(i,j,k) = g_ss(i,j,k)/(1+Is(i,j,k)/Isat(k));
            if i+1<=length(L)
                Is(i+1,j,k) = Is(i,j,k)*exp(g(i,j,k)*delZ);
            end
        end
    end
end

%%Backward
n0back(1,:) = 1;
IpBack = flip(Ip);
IsBack = flip(Is);
for k = 1:length(Is_in)
    for j = 1:length(Ip_in)
        for i = 1:length(L)
            W03back(i,j,k) = cross03*IpBack(i,j,k)/(h*nu_p);
            W02back(i,j,k) = cross02*Is(i,j,k)/(h*nu_s); % 1->2 pump
rate
            W20back(i,j,k) = cross20*IsBack(i,j,k)/(h*nu_s); % 2->1
pump rate
            n2back(i,j,k) =
W03back(i,j,k)/(W03back(i,j,k)+W20back(i,j,k)+1/A20);
            n0back(i,j,k) = 1-n2back(i,j,k);
            g_ssback(i,j,k) = overlap*Ntot*(cross20*n2back(i,j,k)-
cross02*n0back(i,j,k));
            delZ = L(2)-L(1);
            gback(i,j,k) = g_ssback(i,j,k)/(1+IsBack(i,j,k)/Isat(k));
            if i+1<=length(L)
                IsBack(i+1,j,k) = IsBack(i,j,k)*exp(g(i,j,k)*delZ);
            end
        end
    end
end


Inversion = n2-n0;
InversionBack = n2back-n0back;

%% Convert Signal Intensity to Power
for k = 1:length(Is_in)
    for j = 1:length(Ip_in)
        for i = 1:length(L)
            Ps(i,j,k) = Is(i,j,k)*SignalArea(k);
            PsBack(i,j,k) = IsBack(i,j,k)*SignalArea(k);
        end
```

```
    end
end

%% Total Singal Pass Gain
G = squeeze(Is(length(L),:,:)./Is(1,:,:));
GBack = squeeze(IsBack(length(L),:,:)./IsBack(1,:,:));

%% Roundtrip Gain
roundtrips = [0:1:10];
Gtot = zeros(length(roundtrips),length(Ip_in),length(Is_in));
for k = 1:length(Is_in)
    for j = 1:length(Ip_in)
        for i = 1:length(roundtrips)
            Gtot(i,j,k) = (G(j,k)*GBack(j,k))^roundtrips(i);
        end
    end
end



%%
% PsBack = IsBack*Area;
Pp = Ip*PumpArea;
L = L*1000;


%legendCell = cellstr(num2str(TotalPump', 'Pump=%.3g Watts'));
SignalDiameter = SignalDiameter*10^-3;
legendCell = cellstr(num2str(TotalPump', 'Pump=%.3g W'));
titleCell = cellstr(num2str(SignalDiameter','Signal Diameter = %.3g
mm'));



for i = 1:length(Is_in)
     if length(Is_in)>6
        msg = 'Error occurred: Is_in vector is too long.';
        error(msg)
    end
    H = Is(:,:,i);
    RTGain = Gtot(:,:,i);

    if i ==1
        figure('Name',figureCell{ii},'NumberTitle','off');
        subplot(2,2,i)
        plot(L,H)
        lgd = legend(legendCell,'Location','northwest');
        title(lgd,'Pump Powers')
```

```
    title(sprintf('%s',titleCell{i}));
    xlabel('Position in Slab [mm]')
    ylabel('Signal Intensity [W/m^2]')

    subplot(2,2,i+1)
    plot(roundtrips,RTGain)
    lgd = legend(legendCell,'Location','northwest');
    title(lgd,'Pump Powers')
    title(sprintf('%s',titleCell{i}));
    xlabel('# of Round Trips')
    ylabel('Gain')

end
if i == 2
    subplot(2,2,i+1)
    plot(L,H)
    lgd = legend(legendCell,'Location','northwest');
    title(lgd,'Pump Powers')
    title(sprintf('%s',titleCell{i}));
    xlabel('Position in Slab [mm]')
    ylabel('Signal Intensity [W/m^2]')

    subplot(2,2,i+2)
    plot(roundtrips,RTGain)
    lgd = legend(legendCell,'Location','northwest');
    title(lgd,'Pump Powers')
    title(sprintf('%s',titleCell{i}));
    xlabel('# of Round Trips')
    ylabel('Gain')

end
if i == 3
   figure('Name',figureCell{ii},'NumberTitle','off');
    subplot(2,2,i-2)
    plot(L,H)
    lgd = legend(legendCell,'Location','northwest');
    title(lgd,'Pump Powers')
    title(sprintf('%s',titleCell{i}));
    xlabel('Position in Slab [mm]')
    ylabel('Signal Intensity [W/m^2]')

    subplot(2,2,i-1)
    plot(roundtrips,RTGain)
    lgd = legend(legendCell,'Location','northwest');
    title(lgd,'Pump Powers')
    title(sprintf('%s',titleCell{i}));
    xlabel('# of Round Trips')
    ylabel('Gain')
```

```
end
if i == 4
    subplot(2,2,i-1)
    plot(L,H)
    lgd = legend(legendCell,'Location','northwest');
    title(lgd,'Pump Powers')
    title(sprintf('%s',titleCell{i}));
    xlabel('Position in Slab [mm]')
    ylabel('Signal Intensity [W/m^2]')

    subplot(2,2,i)
    plot(roundtrips,RTGain)
    lgd = legend(legendCell,'Location','northwest');
    title(lgd,'Pump Powers')
    title(sprintf('%s',titleCell{i}));
    xlabel('# of Round Trips')
    ylabel('Gain')


end
if i == 5
    figure('Name',figureCell{ii},'NumberTitle','off');
    subplot(2,2,i-4)
    plot(L,H)
    lgd = legend(legendCell,'Location','northwest');
    title(lgd,'Pump Powers')
    title(sprintf('%s',titleCell{i}));
    xlabel('Position in Slab [mm]')
    ylabel('Signal Intensity [W/m^2]')

    subplot(2,2,i-3)
    plot(roundtrips,RTGain)
    lgd = legend(legendCell,'Location','northwest');
    title(lgd,'Pump Powers')
    title(sprintf('%s',titleCell{i}));
    xlabel('# of Round Trips')
    ylabel('Gain')

end
if i == 6
    subplot(2,2,i-3)
    plot(L,H)
    lgd = legend(legendCell,'Location','northwest');
    title(lgd,'Pump Powers')
    title(sprintf('%s',titleCell{i}));
    xlabel('Position in Slab [mm]')
    ylabel('Signal Intensity [W/m^2]')
```

```
        subplot(2,2,i-2)
        plot(roundtrips,RTGain)
        lgd = legend(legendCell,'Location','northwest');
        title(lgd,'Pump Powers')
        title(sprintf('%s',titleCell{i}));
        xlabel('# of Round Trips')
        ylabel('Gain')

    end
end


end
```

References

[1] Saleh, Bahaa E. A., and Malvin Carl Teich. *Fundamentals of Photonics*. Hoboken: Wiley-Interscience, 2007.

[2] "2μm Laser Advancements: Smaller Packages That Pack a Powerful Punch." Accessed November 11, 2019. https://www.edmundoptics.com/resources/trending-in-optics/2um-lasers/.

[3] Scholle, Karsten, Samir Lamrini, Philipp Koopmann, and Peter Fuhrberg. "2μm Laser Sources and Their Possible Applications." *Frontiers in Guided Wave Optics and Optoelectronics,* January 2010. https://doi.org/10.5772/39538.

[4] Geng, Jihong, and Shibin Jiang. "Fiber Lasers: The 2μm Market Heats Up." *Optics and Photonics News* 25, no. 7 (October 2014): 34. https://doi.org/10.1364/opn.25.7.000034.

[5] Einstein, A. "On the Quantum Theory of Radiation." *The Old Quantum Theory*, 1967, 167–83. https://doi.org/10.1016/b978-0-08-012102-4.50018-8.

[6] Zuclich, Joseph A., David J. Lund, and Bruce E. Stuck. “Wavelength Dependence Of Ocular Damage Thresholds In The Near-Ir To Far-Ir Transition Region: Proposed Revisions To Mpes.” *Health Physics* 92, no. 1 (2007): 15–23. https://doi.org/10.1097/01.hp.0000232188.69779.69.

[7] Paschotta, Rüdiger. “Rare-Earth-Doped Gain Media.” RP Photonics Encyclopedia - rare-earth-doped gain media, trivalent, ions, laser crystals, glasses, neodymium, ytterbium, erbium, thulium, holmium, praseodymium, cerium. RP Photonics, October 24, 2019. https://www.rp-photonics.com/rare_earth_doped_gain_media.html.

[8] Wu, Jianfeng. “Thulium Doped Microsphere Laser and Fiber Laser.” Accessed September 30, 2019. http://hdl.handle.net/10150/195201.

[9] Paschotta, Rüdiger. “Upper-State Lifetime.” RP Photonics Encyclopedia - upper-state lifetime, gain medium, quenching, carrier lifetime. RP Photonics, October 24, 2019. https://www.rp-photonics.com/upper_state_lifetime.html.

[10] Xia, Chun. “Concentration Quenching Effect in Rare-Earth Doped Glasses.” The University of Arizona. Accessed November 11, 2019. http://www.optics.arizona.edu/sites/optics.arizona.edu/files/chun-xia-thesis.pdf.

[11] Ganem, Joseph, Jennifer Crawford, Paul Schmidt, N. W. Jenkins, and S. R. Bowman. “Thulium Cross-Relaxation in a Low Phonon Energy Crystalline Host.” Physical Review B. American Physical Society, December 4, 2002. https://journals.aps.org/prb/abstract/10.1103/PhysRevB.66.245101.

[12] Kurkov, Andrei S, E M Sholokhov, A V Marakulin, and L A Minashina. “Effect of Active-Ion Concentration on Holmium Fibre Laser Efficiency.” *Quantum Electronics* 40, no. 5 (March 2010): 386–88. https://doi.org/10.1070/qe2010v040n05abeh014317.

[13] Fang, Qiang, Wei Shi, Khanh Kieu, Eliot Petersen, Arturo Chavez-Pirson, and Nasser Peyghambarian. “High Power and High Energy Monolithic Single Frequency 2 Mm Nanosecond Pulsed Fiber Laser by Using Large Core Tm-Doped Germanate Fibers: Experiment and Modeling.” *Optics Express* 20, no. 15 (May 2012): 16410. https://doi.org/10.1364/oe.20.016410.

[14] Paschotta, Rüdiger. “Fiber Lasers Versus Bulk Lasers.” RP Photonics Encyclopedia - fiber lasers versus bulk lasers, comparison, fiber optics. RP Photonics, April 23, 2019. https://www.rp-photonics.com/fiber_lasers_versus_bulk_lasers.html.

[15] Varangis, P., G. Du Crest, and M. Osinski. “Transverse Modes in Active Cylindrical Waveguides with Step-Index Profiles.” *Proceedings of LEOS 93*, n.d. https://doi.org/10.1109/leos.1993.379084.

[16] Gloge, D. “Weakly Guiding Fibers.” *Applied Optics* 10, no. 10 (January 1971): 2252. https://doi.org/10.1364/ao.10.002252.

[17] Yang, Zhongmin, Can Li, Shanhui Xu, and Changsheng Yang. *Single-Frequency Fiber Lasers*. Singapore: Springer, 2019.

[18] Wicht, A., N. Strauss, I. Ernsting, S. Chepurov, S. Schiller, P. Huke, R.-H. Rinkleff, and K. Danzmann. “A Widely Tuneable, Narrow Linewidth Diode Laser for Precision Spectroscopy.” *2006 Conference on Lasers and Electro-Optics and 2006 Quantum Electronics and Laser Science Conference*, 2006. https://doi.org/10.1109/cleo.2006.4628655.

[19] Lin, H., R. Tao, C. Li, B. Wang, C. Guo, Q. Shu, P. Zhao, et al. “37 KW Monolithic Narrow Linewidth Single Mode Fiber Laser through Simultaneously Suppressing Nonlinear Effects and Mode Instability.” *Optics Express* 27, no. 7 (2019): 9716. https://doi.org/10.1364/oe.27.009716.

[20] Eidam, Tino, Christian Wirth, Cesar Jauregui, Fabian Stutzki, Florian Jansen, Hans-Jürgen Otto, Oliver Schmidt, Thomas Schreiber, Jens Limpert, and Andreas Tünnermann. “Experimental Observations of the Threshold-like Onset of Mode Instabilities in High Power Fiber Amplifiers.” *Optics Express* 19, no. 14 (2011): 13218. https://doi.org/10.1364/oe.19.013218.

[21] Guo, Guangyan, Yanzhong Chen, Jianguo He, Ye Lang, Weiran Lin, Xiongxin Tang, Hongbo Zhang, Zhijun Kang, and Zhongwei Fan. “Diode-Pumped Large-Aperture Nd:YAG Slab Amplifier for High Energy Nanosecond Pulse Laser.” *Optics Communications* 400 (2017): 50–54. https://doi.org/10.1016/j.optcom.2017.04.032.